2022

Magnetic Field Mapping of 1.3 GHz Superconducting Radio Frequency Niobium Cavities

Ishwari P. Parajuli
Old Dominion University, ipara001@odu.edu

Gianluigi Ciovati
Old Dominion University, gciovati@odu.edu

Jean R. Delayen
Old Dominion University, jdelayen@odu.edu

Alex V. Gurevich
Old Dominion University, agurevic@odu.edu

Original Publication Citation

Parajuli, I. P., Ciovati, G., Delayen, J. R., & Gurevich, A. V. (2022). Magnetic field mapping of 1.3 GHz superconducting radio frequency niobium cavities. In F. Zimmerman, H. Tanaka, P. Sudmuang, P. Klysubun, P. Sunwong, T. Chanwattana, C. Petit-Jean-Genaz, & V.R.W. Schaa (Eds.), *Proceedings of the 13th International Particle Accelerator Conference* (pp. 1319-1322). Joint Accelerator Conferences Website. https://doi.org/10.18429/JACoW-IPAC2022-TUPOTK045

ISBN: 978-3-95450-227-1 ISSN: 2673-5490 doi:10.18429/JACoW-IPAC2022-TUPOTK045

MAGNETIC FIELD MAPPING OF 1.3 GHz SUPERCONDUCTING RADIO FREQUENCY NIOBIUM CAVITIES*

I. Parajuli†, G. Ciovati[1], J. Delayen, A. Gurevich, Old Dominion University, Norfolk, USA
[1]also at Jefferson Lab, Newport News, USA

Abstract

Niobium is the material of choice for building superconducting radiofrequency (SRF) cavities, which are fundamental building blocks of modern particle accelerators. These cavities require a cryogenic cool-down to 2 – 4 K for optimum performance minimizing RF losses on the inner cavity surface. However, temperature-independent residual losses in SRF cavities cannot be prevented entirely. One of the significant contributors to residual losses is trapped magnetic flux. The flux trapping mechanism depends on different factors, such as surface preparations and cool-down conditions. We have developed a diagnostic tool: a magnetic field scanning system (MFSS) using Hall probes and anisotropic magneto-resistance sensors to study the spatial distribution of trapped flux in 1.3 GHz single-cell cavities. The first results from this newly commissioned system revealed that the trapped flux on the cavity surface might redistribute with increasing RF power. The MFSS was also able of capturing significant magnetic field enhancement at specific cavity locations after a quench.

INTRODUCTION

Superconducting radio frequency (SRF) cavities are fundamental building blocks of modern particle accelerators. Niobium (Nb) is an elemental superconductor that is most commonly used to build SRF cavities, which operate at liquid helium temperature, 2-4 K. By operating them at such low temperatures the surface resistance due to quasiparticle oscillation under an RF field can be significantly reduced. However, temperature-independent surface resistance referred to as residual resistance is also present, limiting the maximum achievable quality factor, Q_0, of SRF cavities. There are several contributors to the residual losses [1, 2]. A significant one is magnetic flux trapped on the cavity surface. To understand the contribution of trapped flux on residual resistance a diagnostic tool is in high demand. We have designed, developed, and commissioned a magnetic field scanning system (MFSS) that can be used to study trapped flux in SRF cavities. MFSS was developed to use two types of magnetic field sensors: a) Hall probes and b) Anisotropic magnetoresistive (AMR) sensors. Details about the AMR sensor can be found in references [3-10]. The choice of sensors in the MFSS setup is discussed in Ref. [11]. In this contribution, we will discuss the initial results of the newly commissioned MFSS.

* Work supported by NSF Grant 100614-010. Jlab work is supported by Jefferson Science Associates, LLC under U.S. DOE Contract No. DE-AC05-06OR23177.
† ipara001@odu.edu.

EXPERIMENTAL SETUP AND PROCEDURE

Figure 1(a) shows the experimental setup of MFSS. It consists of two brackets supported by a rotating gear system. The gear system is driven by a stepper motor connected to a rotary feedthrough outside the cryostat and allows moving the brackets one full turn in either direction around the cavity. Limit switches are installed to determine the initial and final positions. The angular resolution of the system is 6.8×10^{-3} degrees, corresponding to 13 µm. The initial design of the MFSS made use of a cryogenic stepper motor on each bracket to allow moving the sensors along the cavity contour in the vertical direction [12]. However, the movement of the sensors below ~100 K was unreliable, and we opted for a fixed number of sensors in each bracket. One bracket holds eight Hall probes (HPs) as shown in Fig. 1(c), such that they can measure the radial magnetic field

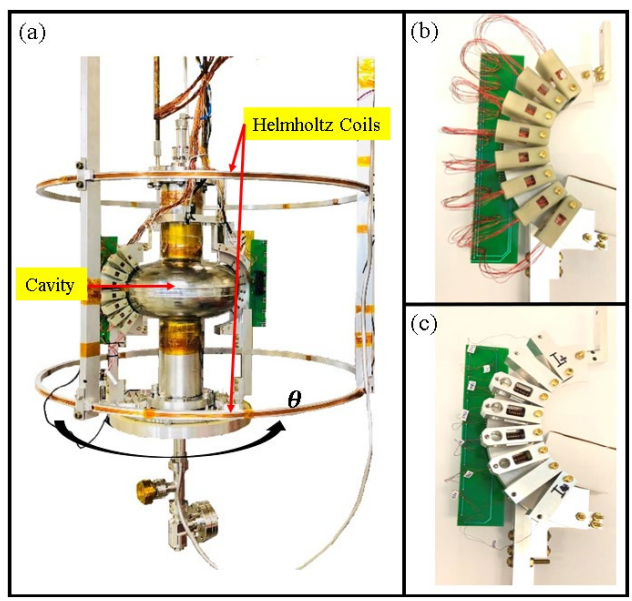

Figure 1: MFSS setup assembled on a 1.3 GHz niobium cavity along with Helmholtz coils (a), AMR sensors attached on a bracket (b), and Hall probes attached on another bracket (c).

on the cavity surface. The other bracket consists of sixteen AMR sensors as shown in Fig. 1(b). Out of sixteen AMR sensors, eight AMR sensors can detect the tangential component of the magnetic field (AMRt), and the remaining eight can measure the radial component of the magnetic field on the cavity surface (AMRr). Each AMRr sensor is ~3 mm away from the corresponding AMRt sensor. The sensors are located in the high RF magnetic field region of the cavity, with sensor No. 1 being the farthest below the

ISBN: 978-3-95450-227-1 ISSN: 2673-5490 doi:10.18429/JACoW-IPAC2022-TUPOTK045

equator and sensor No. 8 being the farthest above the equator. The sensors make a spring-loaded contact with the cavity, in order to measure the magnetic field at the cavity surface. To measure Hall voltage from Hall probes, an 8-channel, 24-bit data acquisition module (USB2AD, AREPOC, Slovakia) was used, whereas a 16-channel data acquisition unit (model 2701 digital multimeter with a model 7701 low-voltage multiplexer, Keithley Instruments, USA) was used to measure the voltage from the AMR sensors. More details about both sensors can be found in reference [11].

The experimental procedure was as follows:

- Prepare the cavity and assemble it in the cleanroom.
- Assemble the MFSS on the cavity and cool to ~10 K > T_c. Measure sensors offset voltages in low ambient DC magnetic field, B_a ~ 3 mG.
- Apply B_a up to 115 mG with Helmholtz coils and cool down to 4.3 K with ΔT~5 K along the cavity axis ("fast" cool-down) or ΔT~0.15 K along the cavity axis ("slow" cool-down).
- After the cavity is immersed in LHe, reduce B_a to ~0.5 mG and measure a magnetic field map of the cavity surface ("B-scan").
- Reduce the He bath temperature to 2 K, while measuring $Q_0(T)$ at a low RF field.
- Measure a baseline B-scan at 2 K with no RF field in the cavity.
- Measure $Q_0(E_{acc})$ at 2 K and perform a B-scan at 5 MV/m, 20 MV/m, and close to the maximum E_{acc}.

RESULTS

The cavity being tested is a 1.3 GHz single-cell cavity of the TESLA shape [13], made of high purity large-grain Nb. Eight RF tests were conducted during this study, four after slow cool-down, and four after fast cool-down.

Figure 2 shows the plots of residual resistance versus applied magnetic field. Following Eqs. (2) and (3) of Ref. [14], the flux trap sensitivity was found to be 0.28 nΩ/mG, and the trapping efficiency was found to be 29%.

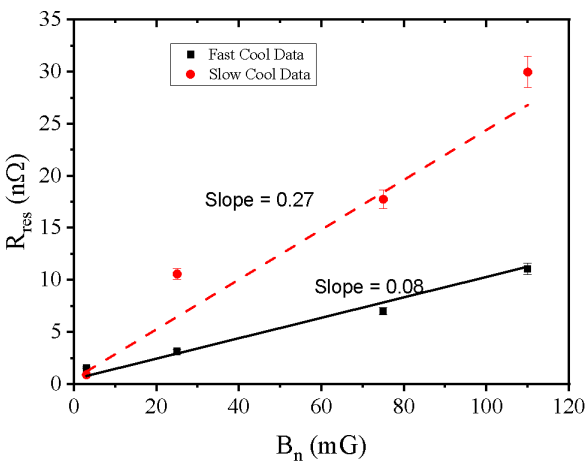

Figure 2: Residual resistance versus applied magnetic field. Solid and dashed lines are weighted linear fits to the corresponding data.

Figure 3 shows Q_0 as a function of the accelerating gradient, E_{acc}. All RF tests were limited by the high-field Q-slope [15, 16] up to ~33 MV/m, corresponding to a peak surface magnetic field of ~136 mT. Multipacting between 18 and 22 MV/m was found in some of the tests. In one instance, (RF test after slow cool with 110 mG), the cavity was quenched during testing due to becoming partly uncovered from the liquid helium. During the quench event, there were no field emission.

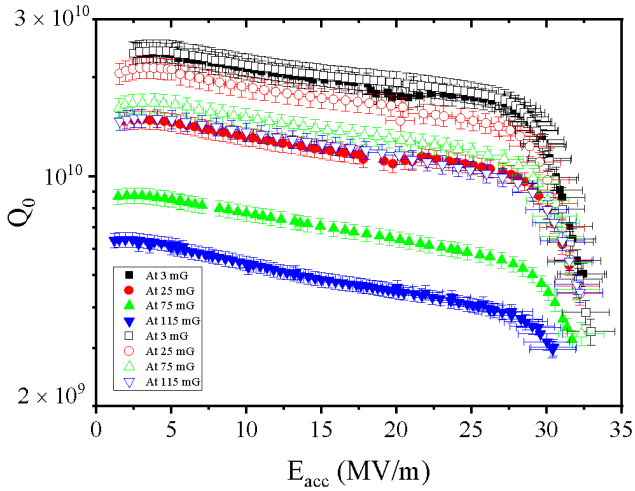

Figure 3: Quality factor (Q_0) versus accelerating gradient (E_{acc}) recorded during high-power RF tests at 2 K after fast cool-down (empty symbols) and after slow cool-down (solid symbols).

The change in a magnetic field (ΔB) relative to the initial value, without any RF field in the cavity at a certain location measured as a function of the peak surface RF magnetic field (B_p/E_{acc} = 4.12 mT/(MV/m)) is shown in Fig. 4.

From Fig. 4, it is clear that the change in the magnetic field (ΔB) varies with changing accelerating gradient.

Figure 5 shows the magnetic field measured by HP8 and AMR8 just after the cavity quenched. At ~325°, all three sensors detected significant enhancement in the magnetic field. We suspect that the location with high trapped flux after quench corresponds to the quench location.

Figure 6 shows the change in magnetic field distribution at 5, 20, and 30 MV/m compared to 0 MV/m. In Fig. 6(d), we see that the magnetic field detected by HP8 near 320° is significantly high after the quench, compared to other parts of the cavity surface and at the beginning of the RF test. Comparing Fig.6 (a), (b), and (c) there seems to be a local re-distribution of the trapped flux with increasing RF field. The average total trapped flux measured by the Hall probes was 81.5 ± 2.3 mG, 81.2 ± 1.8, and 81.7 ± 1.5 mG at 5 MV/m, 20 MV/m, and 30 MV/m, respectively.

ISBN: 978-3-95450-227-1 ISSN: 2673-5490 doi:10.18429/JACoW-IPAC2022-TUPOTK045

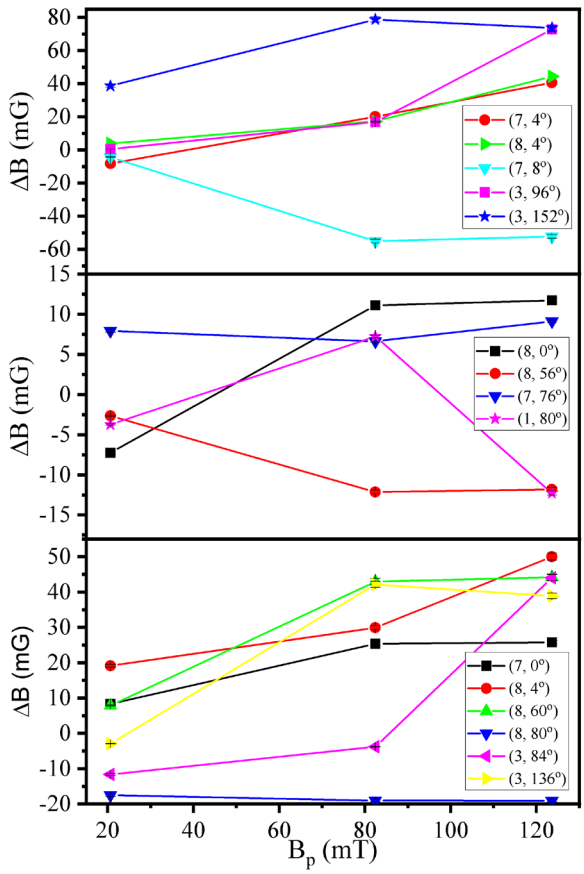

Figure 4: Change in the magnetic field (ΔB) measured by Hall Probes (top plot), AMR radial (middle plot), and AMR tangential (bottom plot) sensors versus B_p at selected locations, identified by the pair (sensor number, θ).

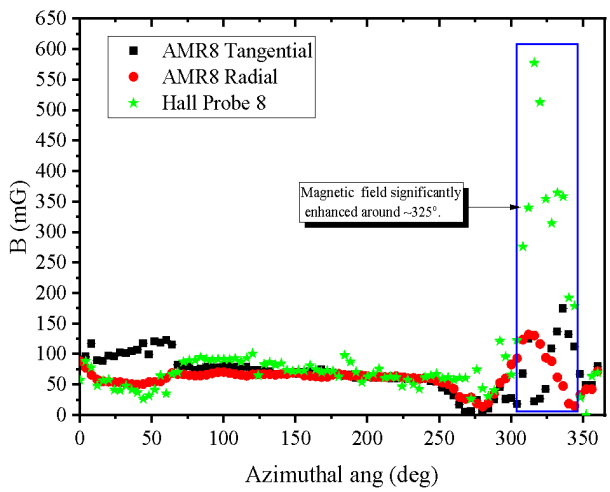

Figure 5: B-field measured by HP8, AMRt8, and AMRr8 along the cavity surface after a quench.

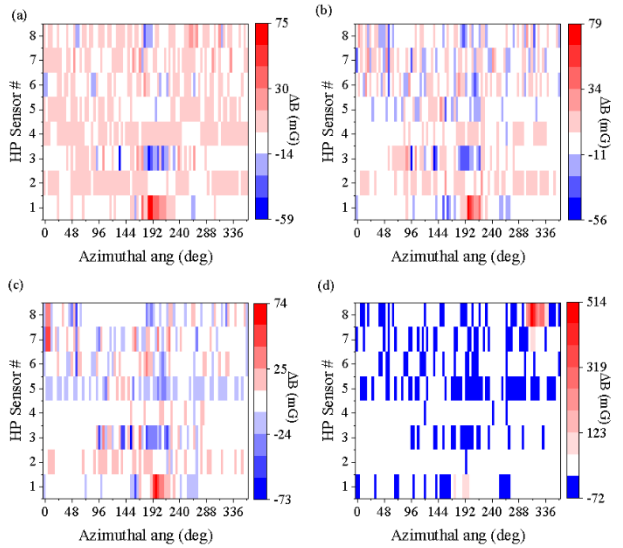

Figure 6: Change in radial magnetic field ΔB measured by Hall probes versus azimuthal angle θ measured at (a) 5 MV/m, (b) 20 MV/m, (c) 30 MV/m, and (d) zero RF power after the quench. The measurements were made at 2 K after a slow cool-down in an applied field of ~115 mG.

CONCLUSION

We have designed, developed, and commissioned a new tool to study trapped flux in SRF single-cell cavities. The initial results of the MFSS applied to a large-grain Nb cavity suggest that the flux trapped at the cavity surface may redistribute with an increasing RF field. Also, most of the trapped flux moved to a specific location of the cavity after the cavity was quenched. In near future, we are planning to perform systematic studies of the different cavities with different treatments.

ACKNOWLEDGEMENTS

We would like to acknowledge JLab SRF staff members for their technical and cryogenic support.

REFERENCES

[1] H. Padamsee, J. Knobloch, and T. Hays, *RF Superconductivity for Accelerators*, Wiley & Sons, New York, 1998.

[2] A. Romanenko, A. Grassellino, O. Melnychuk, and D.A. Sergatskov. J., *Appl. Phys.* 115, 184903 (2014).

[3] I.P. Parajuli, G. Ciovati, J.R. Delayen, and A.V. Gurevich, "Evaluation of Anisotropic Magnetoresistive (AMR) Sensors for a Magnetic Field Scanning System for SRF Cavities", in *Proc. IPAC'21*, Campinas, SP, Brazil, May 2021, pp. 2304-2307. doi:10.18429/JACoW-IPAC2021-TUPAB344

[4] G. Martinet, "Characterization of Small AMR Sensors in Liquid Helium to Measure Residual Magnetic Field on Superconducting Samples", in *Proc. SRF'19*, Dresden, Germany, Jun.-Jul. 2019, pp. 576-579. doi:10.18429/JACoW-SRF2019-TUP058

ISBN: 978-3-95450-227-1 ISSN: 2673-5490 doi:10.18429/JACoW-IPAC2022-TUPOTK045

[5] T. Okada *et al.,* "Systematic evaluation of magnetic sensitivities of anisotropic magnetoresistive sensors at liquid helium temperature for superconducting cavities." *Review of Scientific Instruments* 92.3 (2021): 035003.

[6] R. Ueki *et al.,* "Study on magneto-resistance sensors for low magnetic field measurements," *IEEE Transactions on Applied Superconductivity* 30.4 (2020): 1-4.

[7] B. Schmitz *et al.*, "Magnetometric mapping of superconducting RF cavities," *Review of Scientific Instruments* 89.5 (2018): 054706.

[8] T. Okada *et al.*, "Development of Temperature and Magnetic Field Mapping System for Superconducting Cavities at KEK", in *Proc. SRF'19*, Dresden, Germany, Jun.-Jul. 2019, pp. 583-585. doi:10.18429/JACoW-SRF2019-TUP060

[9] S.N. Lobo, M. Liepe, and T.E. Oseroff, "Magnetic Field Mapping System for Cornell Sample Host Cavity", in *Proc. SRF'19*, Dresden, Germany, Jun.-Jul. 2019, pp. 961-963. doi:10.18429/JACoW-SRF2019-THP046

[10] F. Kramer *et al.*, "Impact of geometry on flux trapping and the related surface resistance in a superconducting cavity," *Physical Review Accelerators and Beams* 23.12 (2020): 123101.

[11] I.P. Parajuli, G. Ciovati, and J. Delayen (2021). Magnetic field sensors for detection of trapped flux in superconducting radiofrequency cavities. *Review of Scientific Instruments*, *92*(10), 104705.

[12] I.P. Parajuli, G. Ciovati, W.A. Clemens, J.R. Delayen, A.V. Gurevich, and J. Nice, "Design and Commissioning of a Magnetic Field Scanning System for SRF Cavities", in *Proc. SRF'19*, Dresden, Germany, Jun.-Jul. 2019, pp. 547-549. doi:10.18429/JACoW-SRF2019-TUP052

[13] B. Aune *et al.*, "Superconducting TESLA cavities." *Physical Review special topics-accelerators and beams* 3.9 (2000): 092001.

[14] P. Dhakal, G Ciovati, and A. Gurevich. "Flux expulsion in niobium superconducting radio-frequency cavities of different purity and essential contributions to the flux sensitivity," *Physical Review Accelerators and Beams* 23, no. 2 (2020): 023102.

[15] P. Kneisel, K. Saito, R. Parodi, "Performance of 1300 MHz KEK-Type Single Cell Niobium Cavities," in *Proc. 8th Workshop on RF Superconductivity*, Abano Terme, Italy, Oct. 1997, paper SRF97C07, pp. 463-471.

[16] E. Kako *et al*., "Cavity Performances in the 1.3 GHz Saclay/ KEK Nb Cavities," in *Proc. 8th Workshop on RF Superconductivity*, Abano Terme, Italy, Oct. 1997, paper SRF97C10, pp. 491-502.